PTBP2 promotes cell survival and autophagy in Chronic Myeloid Leukemia by stabilizing BNIP3

Bibhudev Barik[1,5], Shristi Lama[1,5], Sajitha IS[2], Sayantan Chanda[1,5], Sonali Mohapatra[3], Sutapa Biswas[4], Ghanashyam Biswas[4], Soumen Chakraborty[1,5 *]

[1]Cancer Biology Group, Institute of Life Sciences, Nalco Square, Bhubaneswar, India
[2]Department of Veterinary Pathology, Kerala Veterinary & Animal Sciences University, Wayanad, Kerala, India
[3]Department of Medical Oncology/Hematology, All India Institute of Medical Sciences, Bhubaneswar, India
[4]Sparsh Hospital and Critical Care, Bhubaneswar, India
[5]Regional Centre for Biotechnology, Faridabad, India

***Correspondence to:**
Soumen Chakraborty, Ph.D.
Institute of Life Sciences, Nalco Square, Bhubaneswar, Odisha-751023,
India
Phone: +91-674-2304327
Email : soumen_ils@yahoo.co.in ; soumen@ils.res.in

Keywords : CML, PTBP2, BNIP3, Autophagy, Oxidative Phosphorylation, Imatinib

Running Title: PTBP2-BNIP3 axis promotes autophagy in CML

Abstract

Background

Polypyrimidine tract binding protein 2 (PTBP2) regulates alternative splicing in neuronal, muscle, and Sertoli cells. PTBP2 and its paralog, PTBP1, which plays a role in B-cell development, was found to be expressed aberrantly in myeloid leukemia.

Methods

RNA immunoprecipitation sequencing was used to identify the targets of PTBP2. PTBP2-mediated oxidative phosphorylation and mitochondrial fusion were studied using Seahorse XFp extracellular flux analyzer and confocal microscopy. Athymic nude mice were used to study the role of PTBP2 *in vivo*.

Results

Genetic ablation of Ptbp2 in the cells resulted in decreased cellular proliferation and repopulating ability, decreased ROS, and altered mitochondrial morphology. RNA immunoprecipitation followed by sequencing and functional assays confirmed that PTBP2 binds to Bcl-2 Interacting Protein 3-3'UTR and stabilizes its expression. Our study also suggests that PTBP2 promotes autophagy, as evidenced by the low levels of LC3-II expression in Ptbp2-knockout cells treated with bafilomycin A1. This was restored upon overexpression of Bnip3 in the knockout cells. Finally, we observed that KCL22 cells gave rise to malignant tumors compared to KCL22-Ptbp2 KO cells when injected subcutaneously in the flanks of mice.

Conclusion

PTBP2 promotes cell proliferation and tumor formation while also enhancing autophagy through Bnip3, thus contributing to the progression of CML.

Introduction

Chronic myeloid leukemia (CML) is a type of blood cancer that arises due to a genetic translocation between chromosomes 9 and 22, leading to the expression of a constitutively active tyrosine kinase oncogene called Bcr-Abl1 (**Osman and Deininger, 2021**). The resultant oncoprotein triggers pro-survival signaling pathways in CML cells, providing them with a proliferative advantage and resistance to apoptosis. While tyrosine kinase inhibitors (TKIs) have significantly improved the survival rate of patients with chronic phase CML, the survival rate is much lower for those in the blast phase (**Hochhaus et al., 2017; Jain et al., 2017**). Additionally, most patients require ongoing maintenance therapy for the rest of their lives, as current treatments only suppress the growth of cancer cells. Various BCR-ABL1-dependent and -independent pathways, such as kinase domain mutations, BCR-ABL1 amplification, and aberrant activation of the PI3K and RAS/MAPK signaling pathways, increase the risk of progression and predict poorer response to TKIs (**Melo and Barnes, 2007; Diamond and Melo, 2011; Wagle et al., 2016**). Therefore, identifying the factors responsible for disease progression is crucial to enhance the treatment of CML, particularly in advanced cases. Recent studies have highlighted the crucial role of RNA-binding proteins (RBPs) in cancer by regulating mRNA expression. The polypyrimidine tract-binding protein (PTBP) is one such RBP that plays a critical role in regulating mRNA stability, protein expression, and exon exclusion, thereby influencing cellular growth and development (**Sawicka et al., 2008**). PTBP2, a subtype of PTBP, exhibits differential tissue expression and is correlated with several types of cancer, including glioblastoma, osteosarcoma, and colorectal cancer (**Yang et al., 2014; Ji et al., 2014; Sun et al., 2019; Kim et al., 2021**). Autophagy, a cellular process that maintains cellular balance and prevents the accumulation of impaired proteins and organelles, has also been implicated in tumorigenesis (**Frankel et al., 2017; Abildgaard et al., 2020; Glick, et al., 2010**). Its role in CML is complex, with studies suggesting that it can contribute to both the survival and proliferation of CML cells as well as the development of drug resistance (**Helgason, et al., 2013; Mishima et al., 2008; Bellodi et al., 2009**).

This study investigated the role of PTBP2 in regulating CML pathology and found that it promotes cell proliferation through oxidative phosphorylation (OXPHOS) supported by mitochondrial fusion. Additionally, PTBP2 promotes autophagy by binding and stabilizing Bnip3 RNA, which has been implicated in cancer cell subpopulations and can be a potential therapeutic target. Mice injected with CML Ptbp2 KO cells exhibited significantly smaller tumors and reduced proliferation and autophagy markers, supporting the role of PTBP2 in regulating CML pathology.

Materials and Methods

Cell lines and patient samples

The CML (KCL22, KU812, K562, KYO1, & LAMA84), AML (TF1, HEL, HNT34, & F36P) cell lines and HEK293T cells were cultured in RPMI medium 1640 (Gibco, Cat #31800014) +10% fetal bovine serum (FBS) (Gibco, Cat. #10270106) and Dulbecco's modified Eagle medium (Gibco, Cat. #12100046) respectively, with no antibiotic supplements. Blood samples were collected from CML patients, and the study was approved by the institutional human ethical committee (16/HEC/12).

Generation of stable Ptbp2 KO cell lines

The knockout cell lines were produced by transducing specific sgRNAs for Ptbp2 exon 1 (Horizon, Cat. #VSGH11936-247759039) and exon 2 (Horizon, Cat. #VSGH11936-2430473) in KCL22, KU812, and TF1 cell lines. The Edit-R All-in-one Lentiviral sgRNA non-targeting control viral particles (VSGC11954, Horizon, USA) was used to obtain the

control cells. The clonal selection was performed in those transduced cells, and RT-qPCR and western blotting confirmed PTBP2 knockout.

Generation of stable cell lines overexpressing PTBP2 and BNIP3

The study used lentivirus-based precision lentiORF PTBP2 w/stop codon to overexpress Ptbp2 (Horizon, Cat. #OHS5899-202618163) in LAMA84 cells. For control cells, lentivirus-based precision LentiORF positive control (Horizon, #OHS5833) was transduced into LAMA84 cells and selected with blasticidin. For overexpression of Bnip3, the coding region of Bnip3 was cloned into a lentivirus vector; lentivirus particles were produced by transfecting target plasmid into HEK293T cells, sorting GFP-positive cells and transducing the same in PTBP2 knockout cells.

The expression of PTBP2 was checked by using RT-qPCR (supplementary methods)

Western blotting

Cell protein lysates were obtained using radioimmunoprecipitation assay buffer (RIPA) (Cell Signalling Technology (CST), Cat. #9806). We used 30-50μg of cell lysate with DTT sample loading buffer, resolved them in a sodium dodecyl sulfate-polyacrylamide gel, and transferred them onto an Immobilon-P polyvinylidene fluoride membrane (Merck, Cat. #IPVH00010). Blots were probed with the indicated primary antibodies and horseradish peroxidase-conjugated secondary antibodies. For blot development, Amersham™ ECL™ Prime Western blotting Detection Reagent (GE Healthcare, Cat. #RPN2232) on a Chemidoc™ MP Imaging System (Bio-Rad, USA). The primary antibodies used in this study were anti-GAPDH (Cat. #2118S) and PTBP2 (Cat. #15719) and BNIP3 (Cat. #44060S), and LC3B (Cat. #3868S), ATG7 (Cat. #8558T), ATG12 (Cat. #4180), Beclin-1 (CST, Cat. #3495T), and MFN2 (Cat. #11925), DRP1 (CST, Cat. #8570), TOM20 (CST, Cat. #42406), Bcl-2 (CST, Cat. #15071), and Optineurin (Cat. #79028) and normal Rabbit IgG (CST, Cat. #2729S), and secondary mouse antibody (Cat. #7076), and secondary rabbit antibody (Cat. #7074).

RNA immunoprecipitation

Briefly, 30×10^6 cells were taken and fixed with 0.75% formaldehyde. After fixation, cells were spun down and re-suspended in a buffer comprising protease and RNase inhibitors. The suspension was then incubated on ice for 15 mins, followed by centrifugation at 4^oC. Lastly, the pellet was re-suspended in RIP cross-linked lysis buffer (RCB) and incubated on ice, followed by sonication to prepare the lysate. The prepared lysate was split into two fractions, and antibodies (PTBP2 in one fraction & IgG in another) were added, followed by protein G beads (Millipore, Cat. #16-266) to the immuno-complex for 2h. The co-precipitated RNAs were isolated and sequenced (Supplementary methods).

Cell proliferation assay

Five hundred thousand cells were seeded in a T25 flask in 7ml of RPMI+10% FBS for each group, and the culture was maintained for four days. Each day, the cells were counted independently three times using a Trypan blue solution (Sigma-Aldrich, Cat. #T8154) for each group for the number of viable cells, and their average was considered. A clonogenic assay was conducted, as mentioned in the supplementary methods.

Measurements of OCR and ECAR

The oxygen consumption rate (OCR) and Extracellular Acidification Rate (ECAR) were measured using a Seahorse XFp extracellular flux analyzer (Agilent Technologies, USA). Before the experiment, the XFp-mini plate was coated with 100μl per well of poly-L-lysine and left for at least 45 min at 37°C. Each well was washed with Milli-Q water and dried for at least 1h. 1.25×10^5 KCL22 NTC and Ptbp2 KO cells were seeded in each well in 180μl of XF RPMI Assay Medium (Seahorse Bioscience, Cat. #103576–000) supplemented either with 2mM L-glutamine (Cat. #P0480100) for ECAR measurement or 1mM Sodium-pyruvate (Gibco, Cat. #11360-070), 10mM glucose (Gibco, Cat. #A24940-01), 2mM L-

glutamine for OCR analysis, as per the manufacturer's instructions. The plate was centrifuged and left to equilibrate for 60 min in a CO_2-free incubator before being transferred to an XFp extracellular flux analyzer (Agilent technology, USA). Mitochondrial membrane potential (MMP), cell viability assay, and ROS production assay were conducted as mentioned in the supplementary methods.

Autophagy detection assay

Per the manufacturer's instruction, autophagy detection was performed using CYTO-ID green detection reagent 2 (Enzo Life Sciences, Cat. #ENZKIT175). Briefly, cells were treated with chloroquine or rapamycin for 20h, then centrifuged, rinsed, and suspended in an assay buffer with 5% FBS. Diluted CYTO-ID green was added to each sample, incubated, and analyzed using flow cytometry.

Animal study

All animal protocols were performed with the approval of the ethics committee of the Institute of Life Sciences (ILS/IAEC-130-AH/AUG-18). Cells were injected subcutaneously into the lower flank of 4-6-week-old nude mice. Tumor growth was monitored, and volumes were measured every three days from the second week. Five weeks after injection, mice were sacrificed, and tumor weight was measured and analyzed. Tumors were fixed in 10% neutral buffered formalin for the Hematoxylin & eosin and IHC examination. All studies involved five mice per group. Immunohistochemistry was conducted per the standard protocol and is mentioned in the supplementary methods.

Statistical analysis

The study used ImageJ software for protein band quantification from immunoblotting, GraphPad Prism 9.0 for data analysis, and a two-tailed unpaired student t-test for group comparisons. OCR and ECAR data were analyzed using WAVE 2.6.3. Statistical significance was determined at $p < 0.05$, ***, $p < 0.001$, and $p < 0.001$, and all experiments were repeated at least twice with biological repeats. All data are represented as mean ± SEM.

Results

Establishment and characterization of PTBP2 knockout CML and AML cells

In this study, we examined PTBP2 expression in CML and AML cell lines. The expression of PTBP2 was nearly identical in the four CML cell lines, KCL22, K562, KU812, and KYO1 (**Fig. 1A**). In one CML cell line, LAMA84, PTBP2 expression was found to be reduced (**Fig. 1A**). TF1 (human erythroleukemia), HEL (human erythroid leukemia), and F36P (MDS-RAEB) showed varying levels of PTBP2 expression, whereas HNT34 (BCR-ABL1+ human Acute Myeloid Leukemia) showed almost no PTBP2 expression among the four AML cell lines (**Fig. 1A**). The Cancer Genome Atlas database revealed that PTBP2 expression was higher in patients with AML than in normal **(supplementary Fig. 1A)**. Additionally, a negative relationship between increased PTBP2 expression and the overall survival of 173 AML patients was observed (http://gepia.cancer-pku.cn/) (**supplementary Fig. 1B**).

Next, we assessed cell proliferation and colony formation ability in soft agar by ablating Ptbp2 in CML and AML cells. Previously, we reported that the knockdown of Ptbp2 facilitated the reduction in cellular growth and increased apoptosis **(Nandagopalan et al., 2019**). Herein, Ptbp2 knockout (KO) was achieved using two distinct gRNAs, as outlined in the Materials and Methods section, and several single-cell knockout clones for each cell line were generated and propagated. Using RT-qPCR and western blotting, we confirmed the extent of Ptbp2 knockout in KCL22, KU812, and TF1 cells (**supplementary Fig. 1C and D, and Fig. 1B**). Additionally, Ptbp2 overexpression was confirmed in the LAMA84 cells (**supplementary Fig. 1E and Fig. 1C**). To determine the proliferation rate of the cells, we conducted a trypan blue dye exclusion test on both NTC and Ptbp2 KO KCL22, KU812 cells,

and Ptbp2 overexpressed LAMA84 cells against the vector control. As previously noted, the growth rate was decreased in the KCL22, KU812, and TF1 knockout clones (**Fig. 1D and supplementary Fig. 1F**). An increase in the proliferation rate was observed upon overexpression of Ptbp2 in LAMA84 cells (**Fig. 1E**). Furthermore, the colony count was lower in the Ptbp2 KO KCL22, KU812, and TF1 cells than in the NTC cells (**Fig. 1F and supplementary Fig. 1G**). PTBP2 overexpressed LAMA84 cells showed a higher number of colonies than vector control cells (**Fig. 1G**). The bar graphs shown in Fig. 1F and 1G and supplementary Fig. 1G indicate a significant change in the colony count.

Although imatinib has revolutionized CML treatment, in cases where patients do not respond well or develop resistance, second-generation TKIs, such as dasatinib and nilotinib, are used. A significant decrease in the IC50 value was observed upon imatinib treatment in KCL22 Ptbp2 KO cells compared to the NTC cells; however, treatment with dasatinib and nilotinib showed no significant changes (**Fig. 1H and supplementary Fig. 1H**). After 48h of drug exposure, the IC50 values of imatinib were 0.480 and 0.167μM in KCL22 NTC and KCL22 Ptbp2 KO cells, respectively (**Fig. 1H**). In addition, overexpression of Ptbp2 in the LAMA84 cells increased the IC50 value for imatinib to 0.197μM. It was 0.121μM for its vector control **(Fig. 1I).** Our findings indicated that PTBP2 promotes cell viability in CML cells and protects cells from imatinib-mediated cell death.

PTBP2 targets and regulates several genes in CML

PTBP2 functions as an RNA-binding protein and its four RNA-binding domains regulate the pre-mRNA splicing, translation, and stability of target mRNAs. Therefore, we performed RNA immunoprecipitation and sequencing (RIP-seq) in the KCL22 cell line, which endogenously expresses high levels of PTBP2. First, the complex containing PTBP2 protein and its associated RNA was immunoprecipitated with a PTBP2-specific antibody (**Fig. 2A**), and subsequently, RNA sequencing was performed to profile the PTBP2-bound transcripts. Peak calling with RIPSeeker was performed on each IP alignment file, which produced a list of peaks and their corresponding candidate transcripts. Bound transcripts showing the maximum read counts were considered. Combining three biological repeats, we found that 24 mRNAs were enriched in the PTBP2 RNA-IP samples compared to the control IgG-IP samples (**Fig. 2B and 2C**). Gene Ontology Biological Process (GOBP) analysis of these mRNAs was performed to explore the signaling pathways that PTBP2 might control in CML cells. The Cluster Profiler Bioconductor package was used for gene ontology enrichment of UP- and DOWN-regulated genes for all comparisons with a p-value cutoff of less than or equal to 0.05. The top 10 enriched GO terms were visualized as dot plots (**Fig. 2D**). GO analysis identified significant pathways that regulate transmembrane transport, transmembrane ion transport, and membrane potential, which consists of mitochondrial membrane potential. The mRNA candidates observed in this study were Nampt, Bnip3, and Cacnb2. The binding efficiency between the mRNAs and PTBP2 was validated by independent RNA-IP experiments followed by RT-qPCR, confirming the association between PTBP2 and its targets. Of the 24 targets, strong binding efficiency was detected in 11 (**Fig. 2E**). The remaining 13 exhibited no notable changes. Nampt, followed by Bnip3, showed the highest binding efficiency. The expression levels of 24 targets were compared by RT-qPCR between KCL22-NTC and KCL22-Ptbp2 KO cells and are represented in a heat map (**Fig. 2F**). Although the binding affinity of Nampt was the highest, no corresponding change in NAMPT protein expression was detected between KCL22-NTC and KCL22-Ptbp2 KO cells (**Fig. not shown**). Thus, the 2nd top target, Bnip3 (Bcl-2 Interacting Protein 3), was considered, and its role was further explored in the pathology of CML.

PTBP2 stabilizes and regulates Bnip3 in CML cells

The role of the BH3-only protein BNIP3 in cancer is controversial. Increased BNIP3 levels in cancer patients have been linked to good as well as poor prognosis, as BNIP3

contributes to both pro-cell death and pro-survival signals **(Zhu et al., 2013; Singh et al., 2018)**. RT-qPCR (upper panel) and western blot (lower panel) results illustrated that the expression of BNIP3 in KCL22, KU812, and TF1 NTC cells was higher than that in Ptbp2 KO cells (**Fig. 3A and supplementary Fig. 2A**). An increase in the expression of Bnip3 was noted when PTBP2 was overexpressed in LAMA84 cells (**Fig. 3B**). Analysis of a publicly available dataset GSE4170A, showed a positive correlation between Ptbp2 and Bnip3 expression in different phases of CML (chronic phase (CP), accelerated phase (AP), and blast crisis (BC)) (**supplementary Fig. 3B**) (**Radich et al., 2006**). Moreover, as the disease progressed, there was a gradual increase in the expression of both genes. An independent set of CML samples (n=20) also showed a positive Pearson correlation (r) of 0.8538 ($p<0.001$) between Ptbp2 and Bnip3 expression (**Fig. 3C**). Western blot analysis of some patient samples showed the same correlation (**Fig. 3D**). Thus, our study revealed that Ptbp2 strongly correlates with Bnip3 in CML.

As PTBP2 is an RNA-binding protein, and Bnip3 is one of the most enriched targets in RIP sequencing as well as RT-qPCR validation, we wanted to look into the binding site(s) of PTBP2 on Bnip3 mRNA, for which we scanned Bnip3 mRNA using beRBP (https://bioinfo.vanderbilt.edu/beRBP/predict.html). Only one specific PTBP2 binding site (CUUUUCU) was observed in the 3'-UTR, which had a binding score of 0.362 (**Fig. 3E**). As we observed downregulation of Bnip3 in the absence of PTBP2, we speculate that PTBP2 binds to the 3'UTR of Bnip3 to stabilize it. Next, to confirm the binding of PTBP2 to Bnip3, we cloned the predicted site into a luciferase vector. Transfection with recombinant Ptbp2 (kindly gifted by Dr. Miriam Llorian, University of Cambridge, Cambridge, UK) increased the stability of the relative luciferase reporter count compared to the empty vector control. Modification of the binding site (CAAAACA) using site-directed mutagenesis decreased the relative luciferase reporter count, providing evidence that PTBP2 binds to and regulates the stability of Bnip3 (**Fig. 3F**).

PTBP2-mediated oxidative phosphorylation supported by mitochondrial fusion increases cell proliferation

As cell proliferation is directly linked to cellular energy metabolism, we investigated the mitochondrial function (i.e., OCR) and substrate-level phosphorylation via glycolysis (i.e., ECAR) of KCL22 NTC and KCL22 Ptbp2 KO cells and LAMA84 vector control and Ptbp2 OE cells using a Seahorse XFp extracellular flux analyzer. The basal respiration rate and ATP production were 60% and 63% higher in the KCL22 NTC cells compared to the Ptbp2 KO cells respectively (**Fig. 4A**), and 59% and 63%, respectively, lower in the LAMA84 vector control cells compared to the Ptbp2 OE cells (**supplementary Fig. 3A**). The spare respiratory capacity, defined as the difference between maximal and basal respiration, was found to be decreased by 55% in KCL22 Ptbp2 KO cells. Furthermore, a similar decrease in the glycolysis rate was observed in the KCL22 Ptbp2 KO compared to the KCL22 NTC cells (**Fig. 4B**) and decreased in the LAMA84 vector control compared to LAMA84 Ptbp2 OE cells (**supplementary Fig. 3B**). KCL22 Ptbp2 KO and KU812 Ptbp2 KO cells showed decreased intracellular ATP levels (**Fig. 4C and supplementary Fig. 3E**). As expected, intracellular ATP levels increased in LAMA84 Ptbp2 OE cells (**supplementary Fig. 3C**). Thus, our data suggest that PTBP2 activates both oxidative phosphorylation (OXPHOS) and glycolysis. Respiration is essential for cellular proliferation and is correlated with biological aggressiveness. In addition to decreased ATP production and OXPHOS activity, lower levels of mitochondrial ROS were observed in KCL22 Ptbp2 KO, LAMA84 vector control cells and KU812 Ptbp2 KO cells (**Fig. 4D, supplementary Fig. 3D and 3F**), including the membrane potential in the KCL22 Ptbp2 KO cells (**Fig. 4E**). Live cell imaging showed the same results (**supplementary Fig. 3G**). ROS-regulated signaling pathways are

notably upregulated in different types of cancer, leading to cell proliferation, survival, and other factors contributing to cancer onset and progression (**Liou and Storz, 2010**).

Mitochondrial fusion and fission play essential roles in mitochondrial morphology, and recent studies suggest that increased fusion that correlates with increased Mitofusion-2 (MFN2) expression boosts OXPHOS, leading to heightened cell proliferation (**Yao et al., 2019**). Increased expression of MFN2 in KCL22 NTC cells was observed (**Fig. 4F, first panel**). Furthermore, thin and elongated mitochondria were observed under a confocal microscope in several MitoTracker-stained cells (**Fig. 4G, upper panel**). We also examined the expression of dynamin-related protein 1 (DRP1), which drives constriction and fission during mitochondrial division. The KCL22 Ptbp2 KO cells showed higher expression of DRP1, and small and round mitochondria were observed in most of the cells when stained with MitoTracker (**Fig. 4F, middle panel, and 4G, lower panel**). Likewise, an increase in MFN2 expression and a decrease in DRP1 expression was observed in LAMA84 Ptbp2 OE cells in comparison to vector control cells (**supplementary Fig. 4A**). Thin and elongated mitochondria were also observed in the LAMA84 Ptbp2 OE cells. In contrast, the vector control cells showed only small and round mitochondria (**supplementary Fig. 4B, lower and upper panel, respectively**). Thus, PTBP2 allows for mitochondrial fusion, increased OXPHOS, and cell proliferation.

The presence of PTBP2 promotes autophagy through BNIP3

Previous studies have suggested that BNIP3 can bind to Bcl-2 and release Beclin-1. This process promotes autophagy and inhibits apoptosis **(Zhang et al., 2008; Burton et al., 2009)**. In Ptbp2 knockout KCL22 and KU812 cells, the expression of Beclin-1 and Bcl-2 was decreased, whereas it was increased in LAMA84 cells where Ptbp2 was overexpressed (**Fig. 5A and 5B, 1st and 2nd panel**). The transformation of Microtubule-associated Protein 1 Light Chain 3B (LC3B) from its unconjugated state (LC3-I) to a phosphatidylethanolamine-conjugated state (LC3-II) plays a crucial role in the formation of autophagosomes **(Li, et al., 2020).** BNIP3 is primarily located in the mitochondria and has an LC3B interacting region (LIR) that facilitates the removal of mitochondria via autophagy in somatic cells **(Liu et al., 2022)**. ATG7, which plays a role in converting LC3-I to LC3-II, was decreased in KCL22 and KU812 knockout cells (**Fig. 5A, 3rd panel**). LAMA84 Ptbp2 OE cells exhibited an upregulation of ATG7 (**Fig. 5B, 3rd panel**). As BNIP3 is also involved in mitophagy, we examined the expression of mitophagy-related genes Optineurin and TOM20. Optineurin, an autophagy receptor in the parkin-mediated mitophagy pathway, was upregulated in KCL22, KU812 NTC, and LAMA84 Ptbp2 OE cells compared to their counterparts (**Fig. 5A and 5B, 4th panel**), whereas TOM20, whose abnormal expression is considered an indicator of mitophagy, was downregulated in KCL22, KU812 NTC, and LAMA84 Ptbp2 OE cells (**Fig. 5A and 5B, 5th panel)**. PTBP2 and GAPDH expression levels are also shown **(Fig. 5A, 6th and 7th panel, respectively)**. To gauge the activity of autophagic flux, we used bafilomycin A1, an inhibitor of autophagosome-lysosome fusion, and the mTOR blocker rapamycin, which induces autophagy, in both KCL22 NTC and Ptbp2 KO cells. Elevated expression of LC3-II in KCL22 NTC cells was observed compared to that in KCL22 Ptbp2 KO cells after treatment with bafilomycin A1. These results suggested that PTBP2 plays a vital role in the autophagy of CML cells (**Fig. 5C**). Furthermore, we expressed Bnip3 in KCL22 Ptbp2 KO cells to determine the function of BNIP3 (**Fig. 5D**). After treatment with bafilomycin A1, KCL22 Ptbp2 KO-Bnip3 OE cells showed higher expression of LC3-II than LC3-I, which was almost the same as that in KCL22 NTC cells. The LC3-II/LC3-I ratio was analyzed, and as speculated, both NTC and Bnip3 OE cells showed a higher LC3-II/LC3-I ratio than KO cells (**Fig. 5E, 1st panel, lane 6**). A direct role of PTBP2 was observed when LAMA84 Ptbp2 OE cells were used with respect to the vector control (**Fig. 5F, lane 4 with respect to lane 2**). The ratio of LC3-II/LC3-I was much higher in LAMA84 Ptbp2 OE cells than in the vector

control. The patient sample expressing PTBP2 showed LC3-II expression after treatment with bafilomycin A1, whereas in the sample that did not express Ptbp2, even though bafilomycin A1 was treated, LC3-II was absent **(Fig. 5G)**. Chloroquine (CQ), an antimalarial drug, inhibits autophagy by preventing the fusion of autophagosomes with lysosomes and slowing lysosomal acidification. LAMA84 Ptbp2 OE cells, when treated with only chloroquine or in combination with rapamycin, showed higher autophagic flux than the vector control cells in the Cyto-ID assay (**Fig. 5H**). The autophagic flux was reduced in both cell lines when rapamycin was used without chloroquine. Our observations suggest that PTBP2-mediated stabilization of Bnip3 enhances cell survival by promoting autophagy and cytoprotective functions while preventing ATP depletion and excessive ROS production.

KCL22 cells promote tumorigenesis in athymic nude mice

To investigate the effect of PTBP2 *in vivo*, exponentially growing KCL22 NTC, KCL22 Ptbp2 KO, and KCL22 Ptbp2 KO-Bnip3 OE cells were subcutaneously injected into the flanks of athymic nude mice. From the second week, tumors were measured using a digital caliper. The animal study plan is shown in **Fig. 6A**. We observed large tumors in mice injected with KCL22 NTC cells compared to those injected with KCL22 Ptbp2 KO cells (**Fig. 6B, upper and middle panel**). However, the introduction of KCL22 Ptbp2 KO-Bnip3 OE cells resulted in tumors of size between the wild type and Ptbp2 KO cells. Tumor weight and volume were higher in KCL22 NTC cells than in KCL22 Ptbp2 KO and KCL22 Ptbp2 KO-Bnip3 OE cells (**Fig. 6C and 6D**). In addition, a significant decrease in PTBP2, Ki-67, BNIP3, and Beclin-1 expression was observed in the KCL22 Ptbp2 KO cells, as confirmed by IHC (**Fig. 6E**).

In tissue samples derived from the tumors of NTC mice, apparently healthy and actively dividing cells were observed. The cells were arranged in diffuse sheets supported by well-vascularized fibrous tissue septa. Cellular pleomorphism, a characteristic feature of malignancy, was more evident in mice with KCL22 NTC tumors than in tissue samples derived from tumors of KCL22 Ptbp2 KO **(Suppl. Fig. 5A and 5B)**. KCL22 NTC cells showed large blasts with scant to moderate cytoplasm. The nuclei were vesicular, round, oval, or sometimes folded, with finely stippled chromatin, prominent nucleoli, and high mitotic activity. Some cells were very large, with a high nuclear-cytoplasmic ratio and prominent nucleoli. In the KCL22 Ptbp2 KO group, large areas of necrosis were observed with small islands of proliferating neoplastic cells in between. Individual cell necrosis was evident, characterized by highly eosinophilic cytoplasm and loss of nuclei or karyolysis**.** The neoplastic cells in the active areas were mainly a uniform population of immature cells with some intermediate forms and without much pleomorphism. In the KCL22 Ptbp2 KO-Bnip3 OE group, the cells were primarily consistent with a lower mitotic rate than in the NTC group but higher than that in the KO group. The migration of KCL22 NTC cells through the subcapsular sinus and trabeculae into the spleen was observed. However, no migration of cells into the spleen was observed in mice injected with KCL22 Ptbp2 KO **(Suppl. Fig. 5B)**. Thus, high levels of PTBP2 may contribute to developing a more aggressive form of the disease.

Discussion

RBPs, including Musashi2, heterogeneous nuclear ribonucleoprotein H1, hnRNPA1, and others, have been implicated in CML (**Kharas et al., 2010; Zhang et al., 2014; Li et al., 2020; Wang M. et al., 2020; Liu, et al., 2021**). Msi2 expression was significantly increased, followed by Ptbp2 expression, in blast crisis samples compared to other RBPs (**Nandagopalan et al., 2019**). PTBP2 has been associated with oncogenic RNA splicing in various cancers, such as glioblastoma, osteosarcoma, and colorectal cancer **(Xu and Hecht, 2011; Nowak et al., 2011; Ji et al., 2014; Yang et al., 2014; Tang et al., 2023**). Knockdown of both PTBP1 and PTBP2 slowed glioma cell proliferation (**Cheung et al., 2009), and**

PTBP2 null mice died shortly after birth and exhibited misregulation of alternative splicing in genes involved in cytoskeletal remodeling and cell proliferation (Boutz et al., 2007; Licatalosi et al., 2012). We found that the knockout of Ptbp2 in several CML and AML cells reduced proliferation and long-term colony formation ability. We demonstrated that PTBP2 could increase glycolysis and OXPHOS, leading to a more significant proliferation of cells through increased ATP production and possibly elevated macromolecular precursors. **Yao et al., 2019** recently reported that glycolysis and mitochondrial respiration support the proliferation of oncogene-transformed cells, which aligns with our observation. MFN2 is a protein found in the outer membrane of mitochondria that primarily functions as a mitochondrial fusion protein **(Emery et al., 2021; Ding et al., 2015)**. Mitochondrial biogenesis, as assessed by fusion, was increased in CML cells, which was counteracted when Ptbp2 was knocked out. The elongated shape of the mitochondria in KCL22 NTC cells and the presence of MFN2 suggest that excessive fusion of mitochondria drives cell proliferation. DRP1 is the primary regulator of mitochondrial fission. In KCL22 Ptbp2 KO cells, the existence of DRP1 alongside dotted mitochondria suggests excess fission. Increased mitochondrial fission in Ptbp2 conditional KO (cKO) spermatids was shown due to increased DRP1. This leads to differences in the number and shape of mitochondria between WT and Ptbp2 cKO spermatids **(Hannigan et al., 2018***)*.

Mitochondria, the primary source of ROS in most mammalian cells, are typically higher in cancer cells and function as crucial signaling molecules regulating autophagy and tumor development. Several reports indicate that inhibition of autophagy may be a promising approach for the treatment of BCR-ABL-mediated leukemia **(Karvela et al., 2016; Helgason et al., 2011)**. In this study, we demonstrate that PTBP2 binds to a subset of mRNAs with a very high affinity, and BNIP3 was found to be stabilized by PTBP2. Despite its pro-death activity, BNIP3 expression in cancer often predicts an aggressive disease. Upregulation of BNIP3 characterizes cancer cell subpopulations with increased fitness and proliferation (**Zhu et al., 2022)**. We also observed a strong correlation between Ptbp2 and Bnip3 expression in CML patients. Induction of autophagy through BNIP3 in pre-invasive breast cancers provides tumor cells with extra nutrients and promotes tumor progression **(Zhang et al., 2022)**. Mechanistically, the LC3-II/LC3-I ratio decreased when PTBP2 was knocked out and increased when BNIP3 was overexpressed in the knockout cells. A decrease in the expression of Beclin-1 and ATG7 in KO cells was observed, indicating that the overexpression of PTBP2 is beneficial for the survival of CML cells and reveals a connection between mitochondrial BNIP3 and the progression of CML. We previously showed the antagonistic expression of PTBP1 and PTBP2 in CML cells (**Nandagopalan et al., 2019**). Thus, consistent with our findings, the knockdown of PTBP1 (which increases the level of PTBP2) has been reported to lead to autophagy in colorectal and bladder cancer (**Takai, et al., 2017).** Again, the knockdown of PTBP1 caused the transition of LC3-I to LC3-II in breast and bladder cancer cells, while overexpression of PTBP1 reduced the transition of LC3-I to LC3-II (**Takai, et al., 2017; Wang et al., 2018)**. These reports and our data strongly suggest that PTBP2 positively regulates the proliferation of CML cells through the combinatorial action of oxidative phosphorylation and the transition of LC3-I to LC3-II, thereby promoting autophagy. We observed high PTBP2 expression in some AML cases, indicating poor survival. Thus, we speculate that the PTBP2-BNIP3 axis can potentially contribute to the advancement of acute myeloid leukemia by assisting in the heightened metabolism of cancerous cells, thereby promoting proliferation. The formation of large tumors with microscopic features of cellular pleomorphism and anaplasia and increased Ki67 and Beclin-1 expression in mice injected with KCL22 NTC cells in comparison to KCL22 Ptbp2 KO xenografts provide convincing evidence that the presence of PTBP2 simultaneously promotes proliferation and autophagy, leading to aggressive tumor formation. This suggests that

PTBP2 acts as an oncogene in CML and that PTBP2-mediated induction of autophagy through BNIP3 may provide CML cells with extra nutrients and promote further tumor progression. Based on our current and past data, it is worth proposing PTBP2 as a potential biomarker and therapeutic target for controlling CML progression. In addition, PTBP2 protected cells from the clinically approved BCR-ABL1 inhibitor imatinib, as Ptbp2 KO cells that failed to show autophagy were more sensitive to imatinib. Thus, targeting PTBP2-BNIP3-mediated autophagy by genetic ablation of PTBP2 or pharmacological inhibition of PTBP2 can enhance imatinib sensitivity in CML cells.

Figure Legends

Fig. 1 **PTBP2 protein expression in different cell types and phenotypic assessment**
A. PTBP2 protein expression in CML cell lines (KCL22, K562, KU812, KYO1, and LAMA84) (lanes 1-5) & AML cell lines (TF1, HEL, HNT34, and F36P) (lanes 6-9). An equal amount of protein (30µg) was loaded, and GAPDH western blotting was used as an internal loading control. **B**. Western blot analysis of NTC KCL22 and KU812, KCL22 Ptbp2 KO, and KU812 Ptbp2 KO cell lysates probed with the indicated antibodies. The GAPDH antibody was used as an internal loading control. **C**. Western blot of PTBP2 transduced and stably selected LAMA84 (LAMA84 Ptbp2 OE) and vector control cell lysate was probed with the indicated antibody. The GAPDH antibody was used as an internal loading control. **D**. The proliferation rates of KCL22, KU812 NTC, and LAMA84 vector control and KCL22 Ptbp2 KO, KU812 Ptbp2 KO, and LAMA84 Ptbp2 OE cells were evaluated using the trypan blue exclusion test for cell viability. Proliferation rates at 24, 48, 72, and 96h are represented in the line graph. Each point represents the mean and standard deviation of independent triplicates. **E**. LAMA84 vector control and LAMA84 Ptbp2 OE cell proliferation rate were assessed using a trypan blue dye exclusion test for cell viability. Proliferation rates at 24, 48, 72, and 96h are represented in the line graph. Each point represents the mean and standard deviation of independent triplicates. **F**. Soft agar colony formation assay was performed using KCL22, KU812 NTC, KCL22 Ptbp2 KO, and KU812 Ptbp2 KO cells. Colony numbers are represented in the bar graph below the respective Fig. The bar diagram shows the mean value and corresponding standard deviation for the represented data; n=3. *p<0.05 and ***p<0.001. **G**. Soft agar colony formation assay was performed using LAMA84 vector control and Ptbp2 OE cells. Colony numbers are represented in the bar graph below the respective Fig. **H**. Representative graph of % cell viability in KCL22 NTC and Ptbp2 KO cells by MTT assay after treatment with variable imatinib doses. **I.** Representative graph of % cell viability in LAMA84 vector control and LAMA84 Ptbp2 OE cells treated with variable doses of imatinib.

Fig. 2 **RNA immunoprecipitation (RIP) and sequencing and validation of the PTBP2 bound targets. A**. Immunoprecipitation of PTBP2 was performed using a PTBP2 antibody; 10% of the whole cell lysate was used as input lysate (lane 1), lysate immunoprecipitated with PTBP2 antibody (lane 2), lysate immunoprecipitated with IgG as a negative control (lane 3). The blot was probed with a PTBP2 antibody. **B**. Each circle represents the targets obtained from the single RIP-sequence experiment. Three repeats are presented in a Venn diagram. **C**. The common PTBP2-bound targets are represented in the table. **D**. Gene ontology study of common PTBP2 bound transcripts using Cluster profiler Bioconductor package (*p<0.05). The dot color represents the GO term's significance level, and the dot's size represents the number of genes enriched for the term. Color scale and size scale are given as legends. **E**. RT-qPCR analysis of the PTBP2 bound target transcripts showing a fold enrichment with IgG control. **F**. Heat map showing a fold change in relative mRNA expression of the targets in KCL22 NTC and KCL22 Ptbp2 KO cells.

Fig. 3 **PTBP2 binds and functionally regulates BNIP3. A**. Relative expression of BNIP3 was analyzed by RT-qPCR in KCL22, KU812 NTC, and KCL22 Ptbp2 KO, KU812 Ptbp2 KO cells. Whole-cell lysates of KCL22, KU812 NTC, and KCL22 Ptbp2 KO and KU812 Ptbp2 KO cells were collected, immunoblotting was performed with BNIP3 antibody, and GAPDH was used as an internal loading control (bottom panel). **B**. RT-qPCR analyzed the relative expression of Bnip3 in LAMA84 vector control and LAMA84 Ptbp2 OE cells. Whole-cell lysate of LAMA84 vector control and LAMA84 Ptbp2 OE cells were collected, immunoblotting was performed with BNIP3 antibody, and GAPDH was used as an internal loading control (bottom panel). **C**. Ptbp2 and Bnip3 mRNA correlation in CML patient sample (n=20). **D.** Immunoblotting of some patient samples probed with PTBP2, BNIP3, and GAPDH. **E.** Schematic representation of the binding site of PTBP2 in the 3'UTR region of Bnip3 was detected by beRBP software. The binding region is underlined (top), and the site was mutated by site-directed mutagenesis, as represented below. **F**. 3'UTR binding site in Bnip3 & the mutated site was cloned in the luciferase vector, and luciferase assay was performed by transfecting the clone along with wild-type PTBP2 in HEK293T cells. Renilla luciferase was used as an internal control. After 24h, luciferase activity was measured. Data presented are fold change relative to empty vector-transfected cells. The data was analyzed and represented by a bar diagram. $*p<0.05$ and $***p<0.001$.

Fig. 4 **Diminution of PTBP2 results in mitochondrial dysfunction**. **A**. Mitochondrial stress tests of KCL22 NTC vs. Ptbp2 KO cells. The Seahorse XFp Cell Mito Stress test was utilized, and the OCR measurement was examined in cells treated sequentially with oligomycin, FCCP, and rotenone (left panel). The outcomes represent the mean and standard deviation of three separate experiments. Two-way ANOVA was used for statistical analysis and the comparison test (right panel). **B**. The glycolytic ability was measured in KCL22 NTC vs. Ptbp2 KO cells (left panel). The experiments were carried out using the Seahorse XFp Glycolysis Stress test, and the flow chart and bar graph depict the ECAR measurement (right panel). The results represent the mean and standard deviation of three separate experiments. Two-way ANOVA was implemented for statistical analysis, followed by a multiple comparison test. **C**. Intracellular ATP was assessed in KCL22 NTC vs. Ptbp2 KO cells. The ATP luminescence signals were normalized to the quantity of protein (n = 4). **D**. Mitochondrial superoxide distribution was assessed using mitoSOX dye by flow cytometry and displayed by a bar graph in KCL22 NTC vs. Ptbp2 KO cells. **E**. Flow cytometry measurement of MMP using JC-1 dye in KCL22 NTC vs. Ptbp2 KO cells, illustrated by a bar graph $p< 0.05$, ** $p< 0.01$, *** $p< 0.001$ compared to the controls. **F**. Western blot analysis of MFN2 & DRP1 in control KCL22 NTC vs Ptbp2 KO cells. An equal amount of protein (30µg) was used for both cell lines, and GAPDH was used as an internal loading control. **G**. Confocal microscopic image of KCL22 NTC vs. Ptbp22 KO cells using cmxros mitotracker red dye.

Fig. 5 **Regulation of autophagy by PTBP2 in CML cells**. **A**. Western blot analysis of Beclin-1, Bcl-2, ATG7, Optineurin, TOM20, PTBP2 in KCL22 NTC vs. Ptbp2 KO cells (left panel) & in KU812 NTC vs Ptbp2 KO cells (right panel). An equal amount of protein (30µg) was loaded & GAPDH was used as an internal loading control. **B**. Representative immunoblotting analysis of Beclin-1, Bcl-2, ATG7, optineurin, TOM20, PTBP2 in vector control LAMA84 vector control vs Ptbp2 OE cells. **C.** KCL22 NTC & Ptbp2 KO cells were treated with and without bafilomycin A1 (200nM) & rapamycin (100nM) separately for 18h. **D**. Bnip3 was transduced & overexpressed in KCL22 Ptbp2 KO cells. Western blot analysis was performed for BNIP3 in KCL22 NTC, Ptbp2 KO & KCL22 Ptbp2 KO-Bnip3 OE cells by taking an equal amount of protein. GAPDH was considered a loading control. **E**. KCL22 NTC, Ptbp2 KO & KCL22 Ptbp2 KO-Bnip3 OE cells were treated with or without bafilomycin A1 (200nM) for 18h, lysed and immunoblotted for LC3B with an equal amount

of protein (30ug). GAPDH was used as a loading control. The normalized intensity ratio of LC3-II/LC3-I was taken and represented by a bar diagram (lower panel). **F**. Western blot for LC3B was performed in vector control LAMA84 vector control vs. Ptbp2 OE cells treated with or without bafilomycin A1 (200nM) for 18h, and GAPDH was taken as a loading control. The normalized intensity ratio of LC3-II/LC3-I was taken and represented by a bar diagram (lower panel). **G**. Immunoblotting for LC3B was performed in two patient samples treated with or without bafilomycin A1 (200nM) for 18h. **H**. Flow cytometry-based profiling of autophagy in vector control LAMA84 vector control vs. Ptbp2 OE cells was done. Cells were treated or untreated with 0.5µM Rapamycin, 10µM chloroquine (CQ), or both for 20h. After staining with CYTO-ID green detection reagent for 30 mins in the dark, cells were washed and analyzed by flow cytometry. Results were analyzed and represented with a bar diagram.

Fig. 6 **PTBP2 promotes tumor growth**. **A**. Plan of work for the *in vivo* study. Five million respective cells were injected subcutaneously in 4-6 weeks-old female athymic nude mice. After five weeks, the tumor was collected and processed for IHC. In between that, tumor volume was measured twice a week. **B**. Representative tumor images are represented in the mice injected with KCL22 NTC, Ptbp2 KO & KCL22 Ptbp2 KO-Bnip3 OE cells. The experiment was performed two times, with 5 animals in each group, and the Vernier caliper was used to measure the volume. Values were expressed as mean tumor volume ± SEM. **C**. Graphical representation of the tumor weight of each group of mice and the average weight of tumors were represented by scatter plot. t-test was performed to calculate the statistical significance between those groups. *, $p< 0.05$, **, $p< 0.01$, ***, $p< 0.001$. **D**. Rate of tumor progression of KCL22 NTC, Ptbp2 KO & KCL22 Ptbp2 KO-Bnip3 OE groups are represented by calculating the tumor volume each week. Data is represented by a line graph with an error bar. **E**. Representative IHC images showing the PTBP2, BNIP3, Ki67, and Beclin-1 expression pattern in KCL22 NTC, Ptbp2 KO & KCL22 Ptbp22 KO-Bnip3 OE group tumor.

Acknowledgment BB and SL are supported by a fellowship from the Council of Scientific and Industrial Research (CSIR), India. SC was supported by a fellowship from the University Grants Commission (UGC), India. The pCMV PTBP2 plasmid was kindly provided by Dr. Miriam Llorian (University of Cambridge, Department of Biochemistry, Cambridge, UK). The authors would like to acknowledge the help of Mr. Bhabani Sahoo of the Confocal facility, Mr. Paritosh Nath of the Flow Cytometry facility, Dr. Sarita Jena, and Mr. Biswajit Patra of the Animal House facility.

Author contribution BB, SL, and SC* designed the experiments. BB and SL performed the experiments. SC[¥] performed RT-qPCR. SIS performed the H&E staining and interpretation. SM, SB, and GB provided clinical inputs. SC* arranged for funding, supervised the experiments, interpreted the data, and wrote the manuscript. All authors reviewed and approved the final version of the manuscript. SC[¥]: Sayantan Chanda; SC*: Soumen Chakraborty.

Data Access Statement: Research data supporting this publication are available on request.

Funding This work was supported by grant-in-aid provided to SC* as a part of the "Unit of Excellence (UOE)" by the Department of Biotechnology (DBT), Govt. of India (BT/MED/30/SP11239/2015). The Confocal microscope was supported by an infrastructure facility grant by the Department of Biotechnology (DBT), Govt. of India (BT/INF/22/SP28293/2018). BB and SL were supported by a fellowship from the Council of

Scientific and Industrial Research (CSIR), Government. of India. SC[¥] was supported by a fellowship from the University Grants Commission (UGC), Govt. of India.

Ethical approval and consent to participate All animal protocols were approved by the Institute of Life Sciences (ILS/IAEC-130-AH/AUG-18) Animal Ethics Committee. The Institutional Human Ethical Committee approved the study (16/HEC/12), and peripheral blood samples were collected from patients after obtaining written informed consent. All procedures involving human participants were performed according to the ethical standards of the institutional research committee and with the 1964 Helsinki Declaration and its later amendments or comparable ethical standards.

Conflict of interest: The authors declare no conflict of interest.

References

1.Osman AEG, Deininger MW. Chronic Myeloid Leukemia: Modern therapies, current challenges and future directions. Blood Rev. 2021;49:100825.
2.Hochhaus A, Larson RA, Guilhot F, et al. Long-Term Outcomes of Imatinib Treatment for Chronic Myeloid Leukemia. N Engl J Med. 2017;376(10):917-927.
3.Jain P, Kantarjian HM, Ghorab A, et al. Prognostic factors and survival outcomes in patients with chronic myeloid leukemia in blast phase in the tyrosine kinase inhibitor era: Cohort study of 477 patients. Cancer. 2017;123(22):4391-4402.
4.Diamond JM, Melo JV. Mechanisms of resistance to BCR-ABL kinase inhibitors. Leuk Lymphoma. 2011;52 Suppl 1:12-22.
5.Melo JV, Barnes DJ. Chronic myeloid leukaemia as a model of disease evolution in human cancer. Nat Rev Cancer. 2007;7(6):441-453.
6.Wagle M, Eiring AM, Wongchenko M, et al. A role for FOXO1 in BCR-ABL1-independent tyrosine kinase inhibitor resistance in chronic myeloid leukemia. Leukemia. 2016;30(7):1493-1501.
7.Sawicka K, Bushell M, Spriggs KA, Willis AE. Polypyrimidine-tract-binding protein: a multifunctional RNA-binding protein. Biochem Soc Trans. 2008;36(Pt 4):641-647.
8.Kim JH, Jeong K, Li J, et al. SON drives oncogenic RNA splicing in glioblastoma by regulating PTBP1/PTBP2 switching and RBFOX2 activity. Nat Commun. 2021;12(1):5551.
9.Sun J, Xu H, Qi M, Zhang C, Shi J. Identification of key genes in osteosarcoma by meta analysis of gene expression microarray. Mol Med Rep. 2019;20(4):3075-3084.
10.Yang Z, Chen Y, Fu Y, et al. Meta-analysis of differentially expressed genes in osteosarcoma based on gene expression data. BMC Med Genet. 2014;15:80.
11.Ji Q, Zhang L, Liu X, et al. Long non-coding RNA MALAT1 promotes tumour growth and metastasis in colorectal cancer through binding to SFPQ and releasing oncogene PTBP2 from SFPQ/PTBP2 complex. Br J Cancer. 2014;111(4):736-748.
12.Abildgaard MH, Brynjolfsdottir SH, Frankel LB. The Autophagy-RNA Interplay: Degradation and Beyond. Trends Biochem Sci. 2020;45(10):845-857.
13.Frankel LB, Lubas M, Lund AH. Emerging connections between RNA and autophagy. Autophagy. 2017;13(1):3-23.
14.Glick D, Barth S, Macleod KF. Autophagy: cellular and molecular mechanisms. J Pathol. 2010;221(1):3-12.
15.Helgason GV, Mukhopadhyay A, Karvela M, Salomoni P, Calabretta B, Holyoake TL. Autophagy in chronic myeloid leukaemia: stem cell survival and implication in therapy. Curr Cancer Drug Targets. 2013;13(7):724-734.

16.Bellodi C, Lidonnici MR, Hamilton A, et al. Targeting autophagy potentiates tyrosine kinase inhibitor-induced cell death in Philadelphia chromosome-positive cells, including primary CML stem cells. J Clin Invest. 2009;119(5):1109-1123.
17.Mishima Y, Terui Y, Mishima Y, et al. Autophagy and autophagic cell death are next targets for elimination of the resistance to tyrosine kinase inhibitors. Cancer Sci. 2008;99(11):2200-2208.
18.Zhu Y, Chen B, Yan J, et al. BNIP3 Upregulation Characterizes Cancer Cell Subpopulation With Increased Fitness and Proliferation. Front Oncol. 2022;12:923890.
19.Nandagopalan SR, Agatheeswaran S, Vadlamudi Y, et al. PTBP2 exon 10 inclusion is associated with the progression of CML and it is BCR-ABL1 dependent. Int J Biochem Cell Biol. 2019;109:69-75.
20.Zhu Y, Massen S, Terenzio M, et al. Modulation of serines 17 and 24 in the LC3-interacting region of Bnip3 determines pro-survival mitophagy versus apoptosis. J Biol Chem. 2013;288(2):1099-1113.
21.Singh A, Azad M, Shymko MD, et al. The BH3 only Bcl-2 family member BNIP3 regulates cellular proliferation. PLoS One. 2018;13(10):e0204792.
22.Radich JP, Dai H, Mao M, et al. Gene expression changes associated with progression and response in chronic myeloid leukemia. Proc Natl Acad Sci U S A. 2006;103(8):2794-2799.
23.Liou GY, Storz P. Reactive oxygen species in cancer. Free Radic Res. 2010;44(5):479-496.
24.Yao CH, Wang R, Wang Y, Kung CP, Weber JD, Patti GJ. Mitochondrial fusion supports increased oxidative phosphorylation during cell proliferation. Elife. 2019;8.
25.Zhang H, Bosch-Marce M, Shimoda LA, et al. Mitochondrial autophagy is an HIF-1-dependent adaptive metabolic response to hypoxia. J Biol Chem. 2008;283(16):10892-10903.
26.Burton TR, Gibson SB. The role of Bcl-2 family member BNIP3 in cell death and disease: NIPping at the heels of cell death. Cell Death Differ. 2009;16(4):515-523.
27.Li X, He S, Ma B. Autophagy and autophagy-related proteins in cancer. Mol Cancer. 2020;19(1):12.
28.Liu K, Zhao Q, Sun H, et al. BNIP3 (BCL2 interacting protein 3) regulates pluripotency by modulating mitochondrial homeostasis via mitophagy. Cell Death Dis. 2022;13(4):334.
29.Li SQ, Liu J, Zhang J, et al. Transcriptome profiling reveals the high incidence of hnRNPA1 exon 8 inclusion in chronic myeloid leukemia. J Adv Res. 2020;24:301-310.
30.Zhang H, Tan S, Wang J, et al. Musashi2 modulates K562 leukemic cell proliferation and apoptosis involving the MAPK pathway. Exp Cell Res. 2014;320(1):119-127.
31.Wang M, Sun XY, Zhou YC, et al. Suppression of Musashi□2 by the small compound largazole exerts inhibitory effects on malignant cells. Int J Oncol. 2020;56(5):1274-1283.
32.Kharas MG, Lengner CJ, Al-Shahrour F, et al. Musashi-2 regulates normal hematopoiesis and promotes aggressive myeloid leukemia. Nat Med. 2010;16(8):903-908.
33.Liu M, Yang L, Liu X, et al. HNRNPH1 Is a Novel Regulator Of Cellular Proliferation and Disease Progression in Chronic Myeloid Leukemia. Front Oncol. 2021;11:682859.
34.Tang J, He J, Guo H, et al. PTBP2-Mediated Alternative Splicing of IRF9 Controls Tumor-Associated Monocyte/Macrophage Chemotaxis and Repolarization in Neuroblastoma Progression. Research (Wash DC). 2023;6:0033.
35.Xu M, Hecht NB. Polypyrimidine tract-binding protein 2 binds to selective, intronic messenger RNA and microRNA targets in the mouse testis. Biol Reprod. 2011;84(3):435-439.
36. Nowak U, Matthews AJ, Zheng S, Chaudhuri J. The splicing regulator PTBP2 interacts with the cytidine deaminase AID and promotes binding of AID to switch-region DNA. Nat Immunol. 2011;12(2):160-166.

37.Cheung HC, Hai T, Zhu W, et al. Splicing factors PTBP1 and PTBP2 promote proliferation and migration of glioma cell lines. Brain. 2009;132(Pt 8):2277-2288.
38. Boutz PL, Stoilov P, Li Q, et al. A post-transcriptional regulatory switch in polypyrimidine tract-binding proteins reprograms alternative splicing in developing neurons. Genes Dev. 2007;21(13):1636-1652.
39.Licatalosi DD, Yano M, Fak JJ, et al. Ptbp2 represses adult-specific splicing to regulate the generation of neuronal precursors in the embryonic brain. Genes Dev. 2012;26(14):1626-1642.
40. Emery JM, Ortiz RM. Mitofusin 2: A link between mitochondrial function and substrate metabolism? Mitochondrion. 2021;61:125-137.
41. Ding Y, Gao H, Zhao L, Wang X, Zheng M. Mitofusin 2-deficiency suppresses cell proliferation through disturbance of autophagy. PLoS One. 2015;10(3):e0121328.
42.Hannigan MM, Zagore LL, Licatalosi DD. Ptbp2 Controls an Alternative Splicing Network Required for Cell Communication during Spermatogenesis. Cell Rep. 2017;19(12):2598-2612.
43.Karvela M, Baquero P, Kuntz EM, et al. ATG7 regulates energy metabolism, differentiation and survival of Philadelphia-chromosome-positive cells. Autophagy. 2016;12(6):936-948.
44.Helgason GV, Karvela M, Holyoake TL. Kill one bird with two stones: potential efficacy of BCR-ABL and autophagy inhibition in CML. Blood. 2011;118(8):2035-2043.
45. Zhang G, Xu Z, Yu M, Gao H. Bcl-2 interacting protein 3 (BNIP3) promotes tumor growth in breast cancer under hypoxic conditions through an autophagy-dependent pathway. Bioengineered. 2022;13(3):6280-6292.
46. Takai T, Yoshikawa Y, Inamoto T, et al. A Novel Combination RNAi toward Warburg Effect by Replacement with miR-145 and Silencing of PTBP1 Induces Apoptotic Cell Death in Bladder Cancer Cells. Int J Mol Sci. 2017;18(1).
47. Wang X, Li Y, Fan Y, Yu X, Mao X, Jin F. PTBP1 promotes the growth of breast cancer cells through the PTEN/Akt pathway and autophagy. J Cell Physiol. 2018;233(11):8930-8939.

Fig. 1

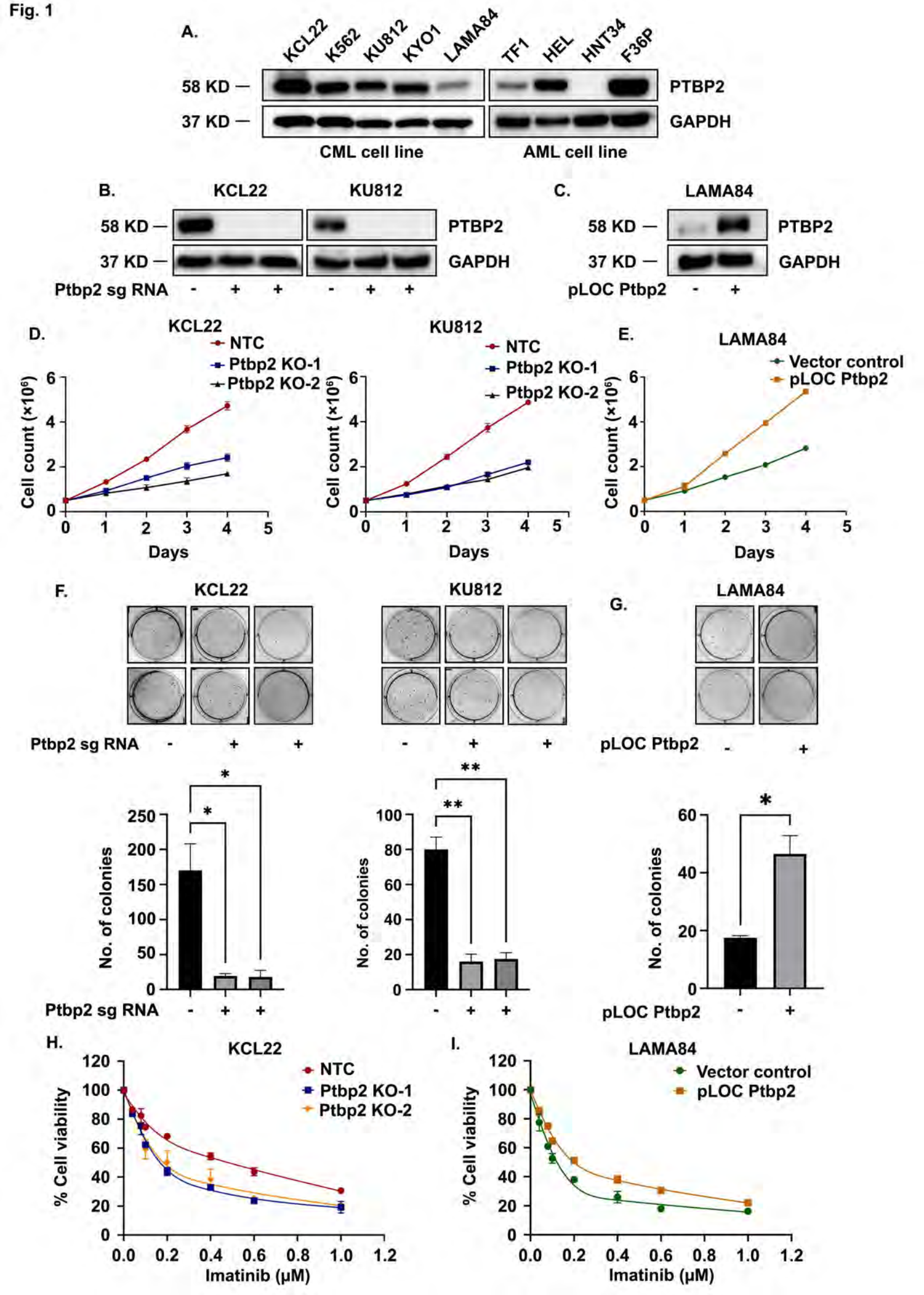
A.
KCL22
K562
KU812
KYO1
LAMA84
TF1
HEL
HNT34
F36P
58 KD
37 KD
PTBP2
GAPDH
CML cell line
AML cell line
B.
KCL22
KU812
Ptbp2 sg RNA
C.
LAMA84
pLOC Ptbp2
D.
NTC
Ptbp2 KO-1
Ptbp2 KO-2
Cell count (×10⁶)
Days
E.
Vector control
pLOC Ptbp2
F.
G.
No. of colonies
H.
% Cell viability
Imatinib (μM)
I.

Fig. 2

A.

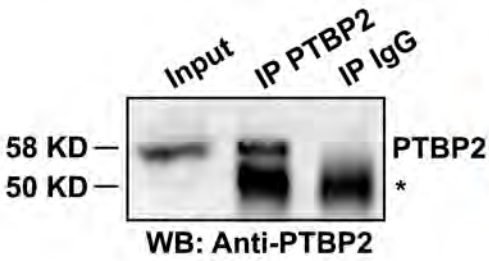

B.

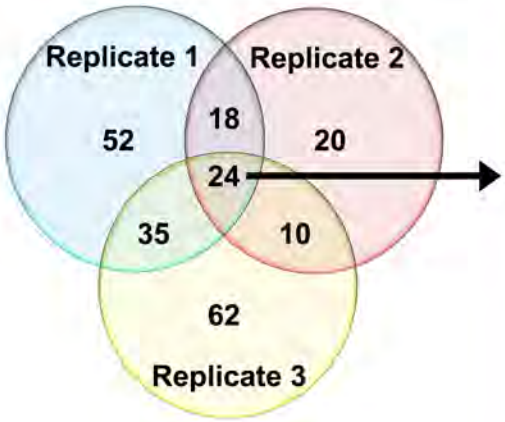

C.

DENR	FAM63B
ACTR2	DKK2
ZNF681	PTP4A1
TWSG1	NAMPT
BBX	CACNB4
UBXN2B	BNIP3
TMEM106B	PSMD11
EMB	CCNI
KLHL28	C6orf25
ERO1L	MCCC2
SLC16A7	PAPOLA
RP3-425C14.4	UBE2V2

D.

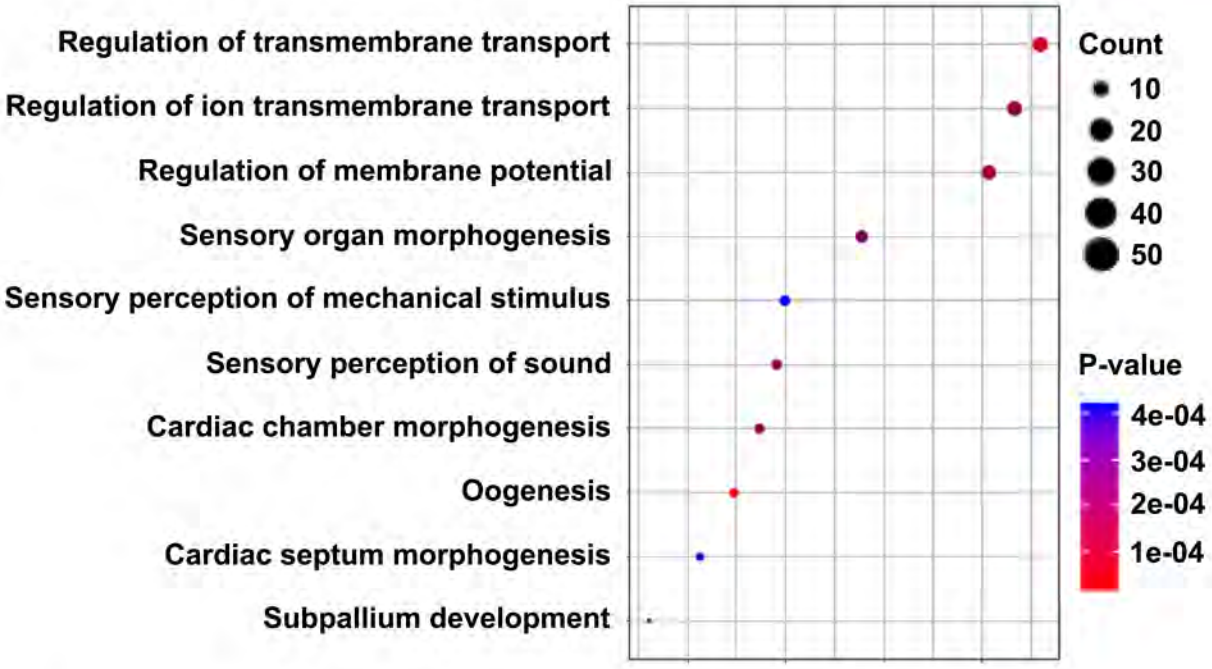

E.

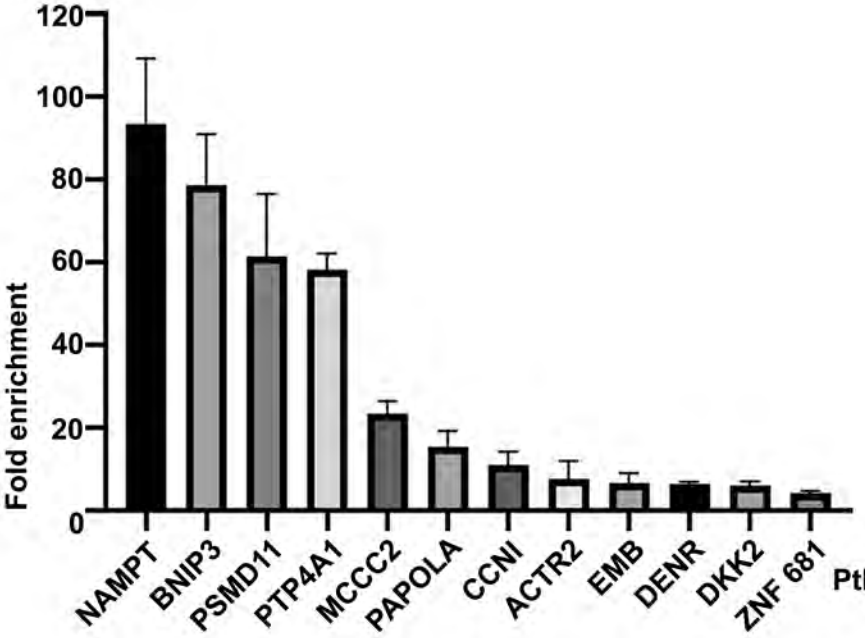

F.

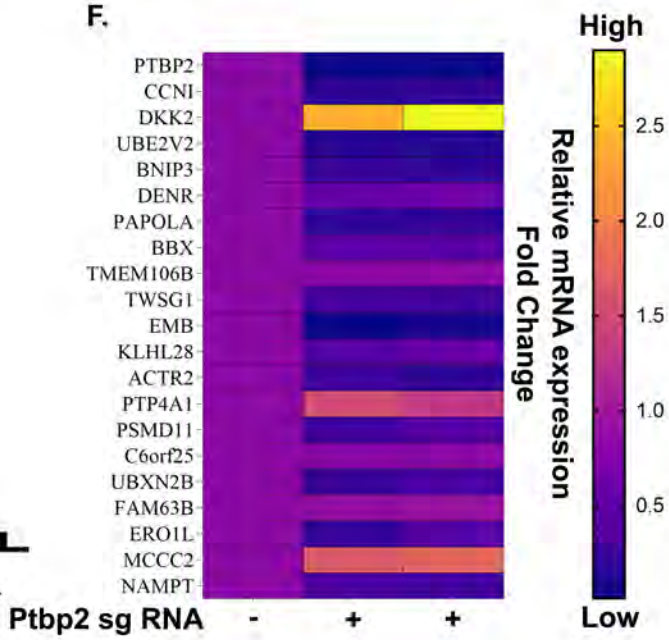

Fig. 3

A.

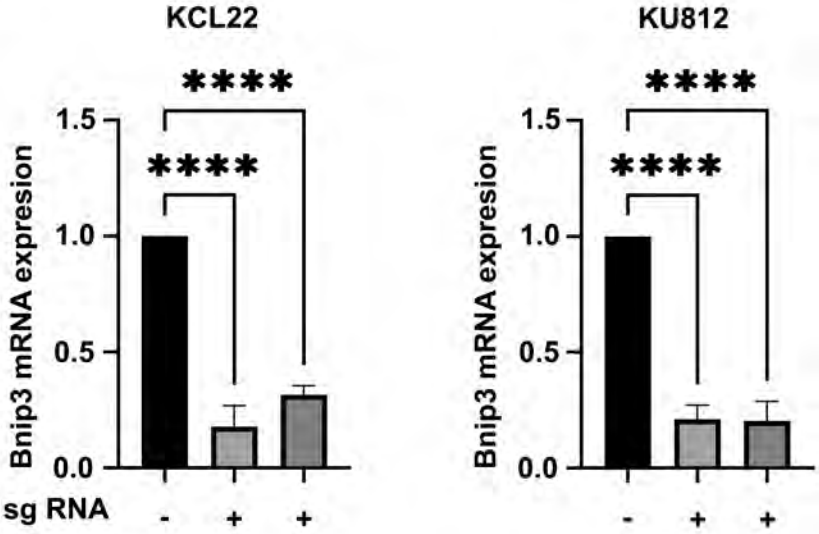

B.

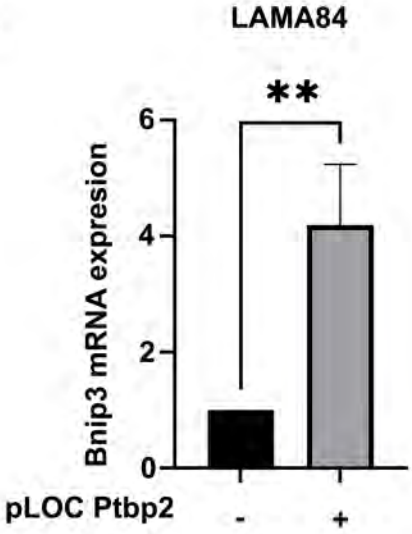

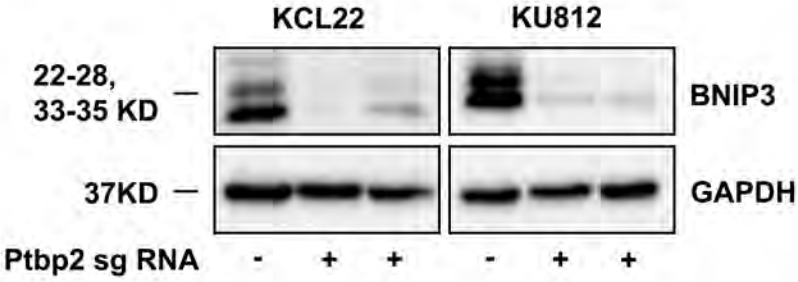

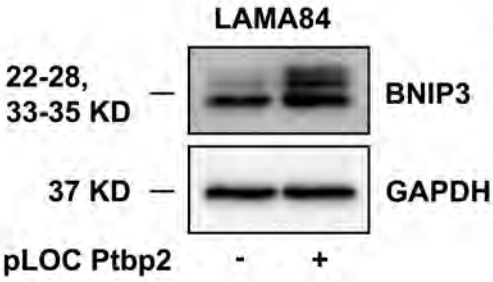

C.

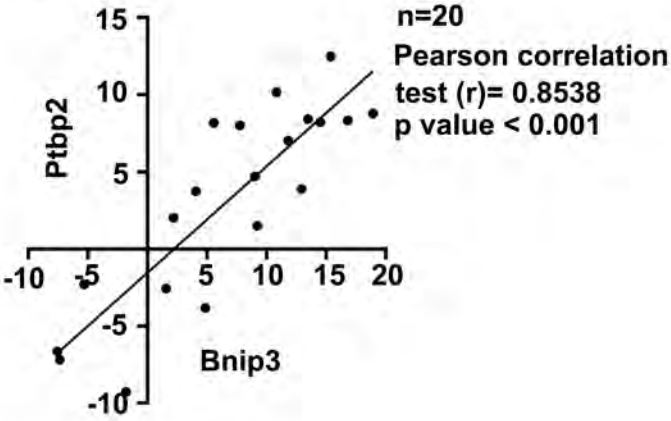

D.

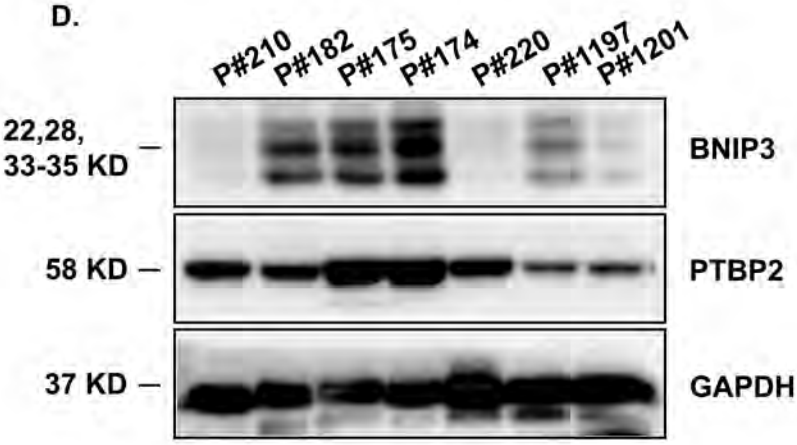

E.

>BNIP3-202 utr3:protein_coding

…UGCCGAAAAGCCUUUUCUGACACUCCUGC…

>BNIP3-202 utr3 Mutated:protein_coding

…UGCCGAAAAGCCAAAACAGACACUCCUGC…

Detail:

seqID	RBP	PWM	motifLen	bindingPos	Score
BNIP3	PTBP2	M227_0.6	7	1612	0.362

F.

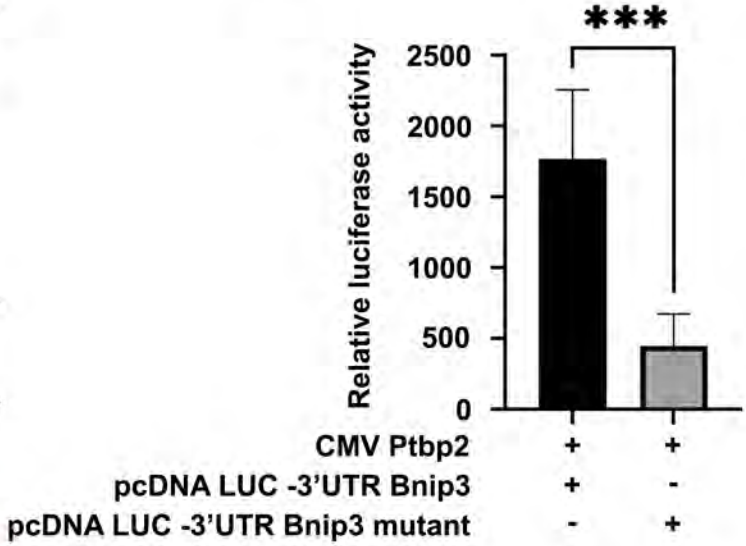

Fig. 4

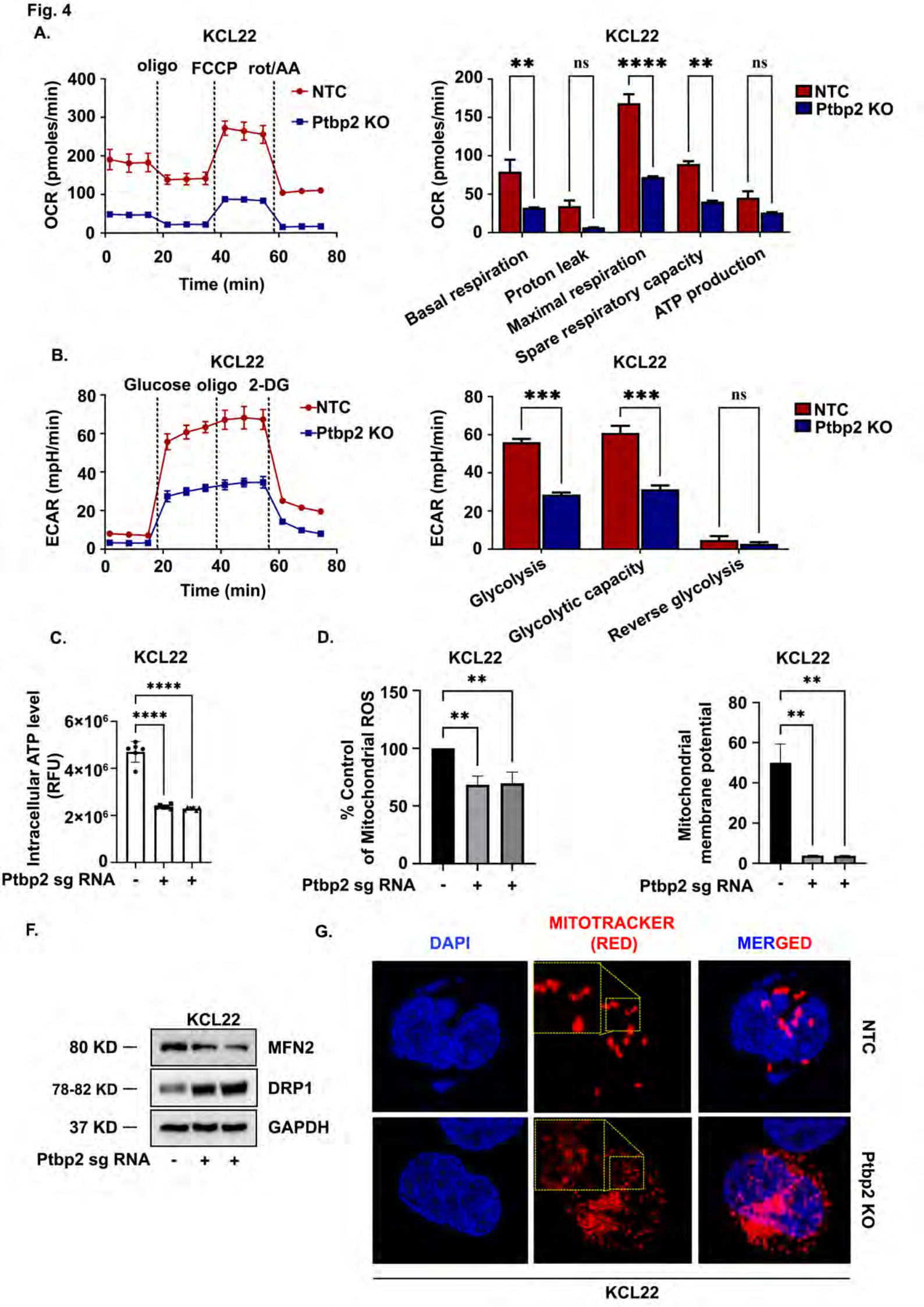
A.
KCL22
oligo
FCCP
rot/AA
NTC
Ptbp2 KO
OCR (pmoles/min)
Time (min)
KCL22
**
ns
****
**
ns
NTC
Ptbp2 KO
OCR (pmoles/min)
Basal respiration
Proton leak
Maximal respiration
Spare respiratory capacity
ATP production
B.
KCL22
Glucose
oligo
2-DG
NTC
Ptbp2 KO
ECAR (mpH/min)
Time (min)
KCL22
***
***
ns
NTC
Ptbp2 KO
ECAR (mpH/min)
Glycolysis
Glycolytic capacity
Reverse glycolysis
C.
KCL22
****
****
Intracellular ATP level (RFU)
Ptbp2 sg RNA
D.
KCL22
**
**
% Control of Mitochondrial ROS
Ptbp2 sg RNA
KCL22
**
**
Mitochondrial membrane potential
Ptbp2 sg RNA
F.
KCL22
80 KD
MFN2
78-82 KD
DRP1
37 KD
GAPDH
Ptbp2 sg RNA
G.
DAPI
MITOTRACKER (RED)
MERGED
NTC
Ptbp2 KO
KCL22

Fig. 5

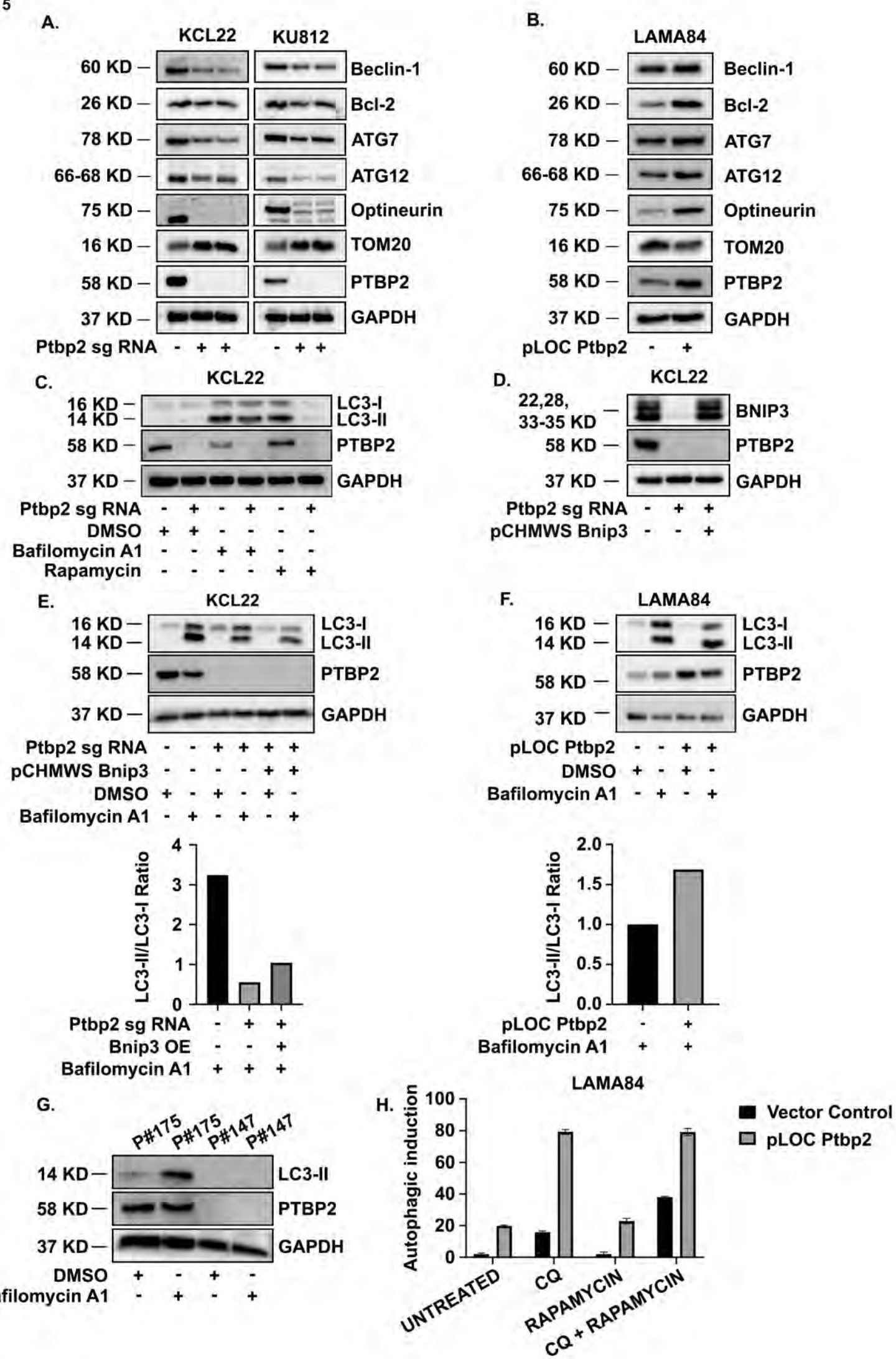
A.
KCL22
KU812
60 KD
26 KD
78 KD
66-68 KD
75 KD
16 KD
58 KD
37 KD
Beclin-1
Bcl-2
ATG7
ATG12
Optineurin
TOM20
PTBP2
GAPDH
Ptbp2 sg RNA - + + - + +
B.
LAMA84
pLOC Ptbp2 - +
C.
KCL22
16 KD
14 KD
LC3-I
LC3-II
Ptbp2 sg RNA - + - + - +
DMSO + + - - - -
Bafilomycin A1 - - + + - -
Rapamycin - - - - + +
D.
22,28,
33-35 KD
BNIP3
Ptbp2 sg RNA - + +
pCHMWS Bnip3 - - +
E.
pCHMWS Bnip3 - - - - + +
DMSO + - + - + -
Bafilomycin A1 - + - + - +
LC3-II/LC3-I Ratio
Bnip3 OE
F.
LAMA84
pLOC Ptbp2 - - + +
DMSO + - + -
Bafilomycin A1 - + - +
G.
P#175
P#175
P#147
P#147
DMSO + - + -
Bafilomycin A1 - + - +
H.
LAMA84
Autophagic induction
Vector Control
pLOC Ptbp2
UNTREATED
CQ
RAPAMYCIN
CQ + RAPAMYCIN

Fig. 6

A.

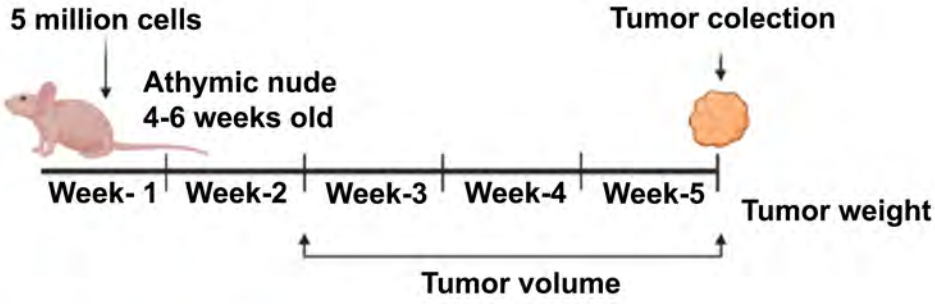
5 million cells
Athymic nude
4-6 weeks old
Tumor colection
Week- 1
Week-2
Week-3
Week-4
Week-5
Tumor weight
Tumor volume

B.

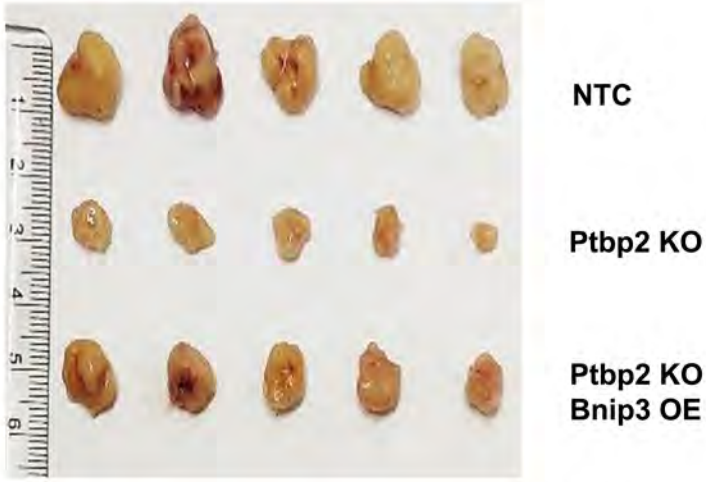
NTC
Ptbp2 KO
Ptbp2 KO
Bnip3 OE

C.

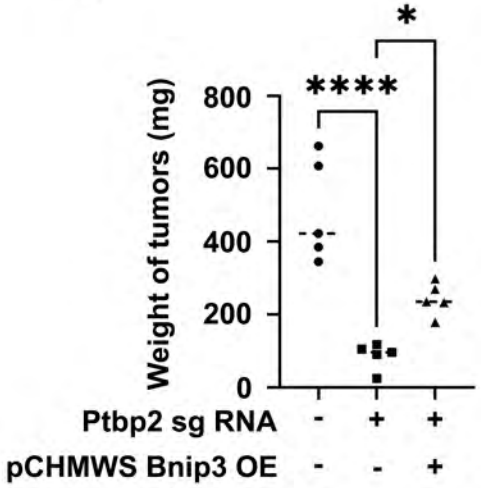
Weight of tumors (mg)
800
600
400
200
0
****
*
Ptbp2 sg RNA - + +
pCHMWS Bnip3 OE - - +

D.

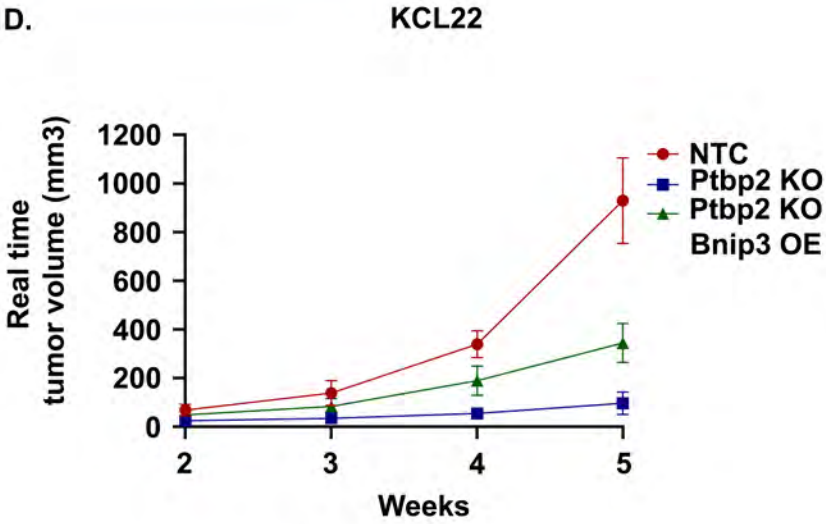
KCL22
Real time
tumor volume (mm3)
1200
1000
800
600
400
200
0
2
3
4
5
Weeks
NTC
Ptbp2 KO
Ptbp2 KO
Bnip3 OE

E.

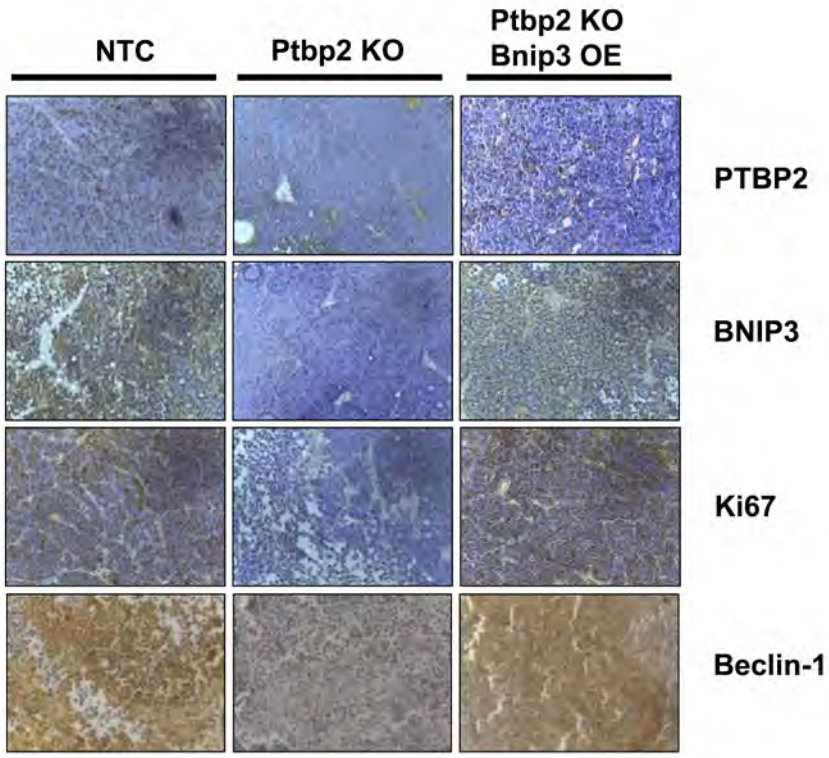
NTC
Ptbp2 KO
Ptbp2 KO
Bnip3 OE
PTBP2
BNIP3
Ki67
Beclin-1